DIRECT MODEL-BASED TOMOGRAPHIC RECONSTRUCTION OF THE COMPLEX REFRACTIVE INDEX

K. Aditya Mohan[*], *Xianghui Xiao*[†], *Charles A. Bouman*[*]

[*]School of Electrical and Computer Engineering, Purdue University, West Lafayette, IN 47907, USA
[†]Argonne National Laboratory, Lemont, IL 60439

ABSTRACT

X-ray propagation-based phase contrast tomography (XPCT) has become popular as a method for tomographically reconstructing the complex refractive index of a material from single distance measurements. XPCT has two major advantages over traditional X-ray computed tomography (CT): It can be used at higher cone-beam magnifications, and it typically produces higher contrast. However, current XPCT reconstruction algorithms are limited to near-field diffraction, which limits both their use and the quality of reconstructions.

In this paper, we present a model-based iterative reconstruction (MBIR) algorithm called complex refractive index tomographic iterative reconstruction (CRITIR). CRITIR is based on a non-linear physics based model for X-ray propagation and a prior model for the complex refractive index of the object being imaged. Unlike conventional methods, CRITIR is designed to work within and beyond the near-field diffraction region. We use simulation to show that our algorithm accurately reconstructs the object while the conventional methods result in inaccurate reconstructions with blurry edges beyond the near-field region.

Index Terms— Phase retrieval, phase contrast, X-ray tomography, complex refractive index, Fresnel diffraction.

1. INTRODUCTION

Traditional X-ray computed tomography (CT) is widely used to reconstruct the X-ray absorption index (i.e., the imaginary part of the refractive index), and it assumes no X-ray diffraction. In practice, X-rays diffract whenever the object to detector distance is large, as happens in cone beam systems at high magnifications. So traditional CT is restricted to lower cone-beam magnifications. Alternatively, X-ray phase contrast tomography (XPCT) has become increasingly popular as a method for tomographic imaging when both diffraction and absorption occur. Moreover, since the contrast in the real part of the index of refraction that is responsible for diffraction is typically orders of magnitude greater than the imaginary part, XPCT typically has much higher contrast than traditional CT.

K. A. Mohan and C. A. Bouman were supported by an AFOSR/MURI grant #FA9550-12-1-0458.

However, existing XPCT reconstruction algorithms have severe limitations [1]. First, all existing XPCT reconstruction algorithms either assume that the object is weakly absorbing [2,3] or that the real part of the refractive index is linearly related to the imaginary part [3–6]. More importantly, existing XPCT algorithms generally assume that the diffraction is weak. For example, the widely used reconstruction algorithms presented in [2, 4–6] assume the near-field condition where only the first order Fresnel diffraction fringe is resolved. These methods result in inaccurate reconstructions with artifacts and excessively smooth edges beyond the near-field region. Other methods allow for more diffraction in the form of higher-order Fresnel diffraction fringes obtained beyond the near-field region [1, 3]. However, they assume that the scattered field is weak in both amplitude and phase [1, 3], which severely limits the variety of samples that can be used for imaging. Nevertheless, these methods are widely used outside the scope of their validity due to the lack of better algorithms for XPCT.

In this paper, we present a model-based iterative reconstruction (MBIR) algorithm called complex refractive index tomographic iterative reconstruction (CRITIR) that does not make simplifying approximations beyond the assumption of Fresnel diffraction. In CRITIR, the reconstruction of the complex refractive index is given by iteratively minimizing a cost function consisting of a forward model term and a prior model term that enforces sparsity in reconstruction. The forward model accounts for both absorption and phase contrast in the measurements by modeling the physics of X-ray interaction with the object and Fresnel diffraction [7]. However, the forward model is highly non-linear due to the loss of phase during measurement and the complex exponential form of attenuation and refraction. To minimize this non-convex cost function, we propose a novel algorithm that uses variable splitting and the method of alternating direction method of multipliers (ADMM) [8] to decompose the original problem into an iterative solution of multiple simpler optimization problems.

2. PROPAGATION MODEL

In this section, we express the X-ray electric field in the detector plane as a function of the complex refractive index that

is defined as [9],

$$n(u,v,w) = 1 - \delta(u,v,w) + j\beta(u,v,w) \quad (1)$$

where $j = \sqrt{-1}$, $\beta(u,v,w)$ is the absorption index, and $\delta(u,v,w)$ is the refractive index decrement of the object at the spatial coordinates (u,v,w). The relation between the X-ray electric field incident on the object, $f_I(u,v)$, and the electric field at the exit plane of the object, $f_O(u,v)$, is [7, 9],

$$f_O(u,v) = f_I(u,v) \exp\left\{ \frac{2\pi j}{\lambda} \int_w [1 - \delta(u,v,w) + j\beta(u,v,w)]\, dw \right\} \quad (2)$$

where λ is the wavelength and w-axis is the direction of X-ray propagation. Note that the absorption index, β, is related to the linear attenuation coefficient, μ, as $\mu = (4\pi/\lambda)\,\beta$. From (2), we can see that the real part of the refractive index modulates the phase whereas the imaginary part, the absorption index, modulates the amplitude of the incident electric field.

In PCXT, the scattering is mainly confined within a small angular range along the direction of propagation. Therefore, paraxial approximation can be safely used in the near-field diffraction regime and beyond. Thus, we use the Fresnel integral to express the electric field in the detector plane, $f_D(u,v)$, as a linear convolution of $f_O(u,v)$ with the Fresnel impulse response [7] as shown below,

$$f_D(u,v) = \frac{j \exp(jkR)}{\lambda R} \int_{u'} \int_{v'} f_O(u',v') \exp\left(\left(\frac{j\pi}{\lambda R} \right) \left[(u-u')^2 + (v-v')^2 \right] \right) du'dv'. \quad (3)$$

where R is the object to detector distance and $k = 2\pi/\lambda$ is the wavenumber. Note that it is sufficient to consider the case of parallel beam since the physics of cone-beam can be expressed in the form of an equivalent parallel beam configuration [7].

The partial coherence of the X-ray electric field limits the achievable spatial resolution. This effect is modeled in Fourier space by multiplying the Fresnel frequency response by a window such as a Gaussian [7]. Thus, the relation between the Fourier transform of $f_D(u,v)$ denoted by $F_D(\mu,\nu)$, and the Fourier transform of $f_O(u,v)$ denoted by $F_O(\mu,\nu)$ is [7],

$$F_D(\mu,\nu) = W(\mu,\nu) \exp(jkR) \exp\left((-j\pi\lambda R)\left(\mu^2 + \nu^2\right) \right) F_O(\mu,\nu) \quad (4)$$

where (μ,ν) are the spatial frequency coordinates in inverse units of (x,y), $W(\mu,\nu) = \exp\left(-(\mu^2+\nu^2)/(2\gamma^2)\right)$, and γ is the standard deviation of the Gaussian window [7].

3. PROBLEM FORMULATION

In MBIR, the reconstruction is given by solving the following optimization problem,

$$\hat{x} = \underset{x \geq 0}{\operatorname{argmin}} \left\{ -\log p(y|x) - \log p(x) \right\} \quad (5)$$

where $\log p(y|x)$ is the forward log-likelihood function for the data, y, given the object x and $\log p(x)$ is the prior log-likelihood function for the object, x.

We first derive the forward likelihood function $p(y|x)$. Let the real part of the vector x give the refractive index decrement and the imaginary part give the absorption index voxel values in discrete space. Then, the electric field in the exit plane of the object is given by numerically evaluating equation (2) as, $D \exp(-A_i x)$, where A_i is the matrix that implements the line integral in (2) at the i^{th} view, D is a diagonal matrix such that the diagonal elements give the incident X-ray electric field, and $\exp(z)$ is element-wise exponentiation of the vector z. Here, the object independent constant phase multiplier in (2) is ignored as it does not contribute to the measurement. In case of plane wave illumination, D is an identity matrix with a fixed multiplicative constant.

The detector response is proportional to the X-ray intensity, which is the magnitude square of the X-ray electric field after it propagates from the object to the detector. The variance in detector count measurements is typically modeled using Poisson statistics [10]. By the variance stabilizing property of the square root transformation for Poisson random variables, we can show that the square root of detector measurements, y_i, is well approximated by a constant variance Gaussian distribution with mean equal to $|HD\exp(-A_i x)|$ where H is the matrix that implements the Fresnel diffraction integral in Fourier space using (4) [11] and $|.|$ gives the element-wise magnitude of a vector. Thus, the relation between the data, y_i, at the i^{th} view and the object, x, is,

$$y_i = |HD\exp(-A_i x)| + n_i \quad (6)$$

where n_i is the noise in data, y_i, at the i^{th} view.

Thus, the forward log-likelihood function of y given x is,

$$-\log p(y|x) = \sum_{i=1}^{M} \frac{1}{2\sigma^2} \left|\left| y_i - |HD\exp(-A_i x)| \right|\right|^2 + g(y) \quad (7)$$

where σ^2 is the noise variance, M is the total number of views, and $g(y)$ is a constant.

Next, we derive the prior log-likelihood function, $\log p(x)$. Typically, there is a strong correlation between the refractive index decrement, $x_j^{(R)}$, and absorption index, $x_j^{(I)}$, values of an object [4, 5] . The transform, T, that decorrelates the real part, $x_j^{(R)}$, and the imaginary part, $x_j^{(I)}$, of the voxel x_j is given by,

$$\begin{bmatrix} x_j^{(+)} \\ x_j^{(-)} \end{bmatrix} = \begin{bmatrix} 1 & \alpha \\ 1 & -\alpha \end{bmatrix} \begin{bmatrix} x_j^{(R)} \\ x_j^{(I)} \end{bmatrix} \quad (8)$$

where α is the ratio of standard deviation of $x_j^{(R)}$ to $x_j^{(I)}$.

In the prior model, we independently regularize the sum component, $x_j^{(+)}$, and the difference component, $x_j^{(-)}$, of x_j using a $26-$point local neighborhood based qGGMRF prior model [12]. The prior model is given by,

$$R(x) = \sum_{i,j \in \mathcal{N}} \rho\left(Tx_i - Tx_j\right) \quad (9)$$

where $\mathcal{N}$ is the set of all pairwise cliques in 3D space and $\rho(\Delta)$ is the potential function given by,

$$\rho\left(\begin{bmatrix}\Delta^{(+)}\\ \Delta^{(-)}\end{bmatrix}\right) = \frac{\left|\Delta^{(+)}/\sigma_+\right|^2}{c+\left|\Delta^{(+)}/\sigma_+\right|^{2-q}} + \frac{\left|\Delta^{(-)}/\sigma_-\right|^2}{c+\left|\Delta^{(-)}/\sigma_-\right|^{2-q}} \tag{10}$$

where $q = 1.2, \sigma_+, \sigma_-$, and c are qGGMRF parameters. The decorrelating transform in (8) and the prior model in (9) can be used to enforce prior knowledge about the object. For instance, if we know that the refractive index decrement, δ, is approximately proportional to the absorption index, β, then we can set $\alpha = \delta/\beta$ and $\sigma_-/\sigma_+ << 1$.

By substituting (7) and (9) in (5), we can formulate the reconstruction as,

$$\hat{x} = \underset{x\geq 0}{\operatorname{argmin}} \left\{ \sum_{i=1}^{M} \frac{1}{2\sigma^2} \left|\left|y_i - \left|HD\exp\left(-A_i x\right)\right|\right|\right|^2 + R(x) \right\} \tag{11}$$

where $-\log p(x) = R(x)$ is the prior model.

The above form of the cost function is non-convex and difficult to minimize directly. To simplify the problem, we will use variable splitting using the auxiliary vectors $w_i = \exp(-z_i)$ and $z_i = A_i x$, and formulate the problem as a constrained optimization problem of the form,

$$(\hat{x},\hat{z},\hat{w}) = \underset{x\geq 0,z,w}{\operatorname{argmin}} \left\{ \frac{1}{2\sigma^2} \sum_{i=1}^{M} \left|\left|y_i - \left|HDw_i\right|\right|\right|^2 + R(x) \right\}$$
$$\text{subject to } w_i = \exp(-z_i) \text{ and } z_i = A_i x \;\forall\, i \tag{12}$$

The above form of constrained optimization problem can be solved using the augmented Lagrangian and the method of alternate direction method of multipliers (ADMM) [8].

4. OPTIMIZATION ALGORITHM

Using ADMM [8], we can solve (12) by iteratively solving multiple but simpler optimization problems shown in algorithm (1). Here u_i and v_i are the scaled dual vectors, $\mu > 0$ and $\nu > 0$ are the augmented Lagrangian parameters, and K_{max} and L_{max} are the maximum number of outer and inner loop iterations respectively.

In algorithm (1), the optimization problem given by (13) is solved using the algorithm in [10, 13–15]. The minimization problem shown in (14) is separable in each element of the vector, z_i, and reduces to multiple 2-dimensional minimization problems (in real and imaginary parts of $z_{i,k}$) that is solved using the Nelder-Mead simplex algorithm [16].

To solve the optimization problem in (15), we will use a diagonal phase matrix Ω_i such that $|\Omega_{i,k,k}| = 1$ to account for the unknown phase of y_i. Thus, we will minimize (15) by solving the alternate optimization problem given by,

$$\left(\hat{w},\hat{\Omega}\right) = \underset{w,\Omega}{\operatorname{argmin}} \frac{1}{2\sigma^2} \left\{ \sum_{i=1}^{M} \left|\left|y_i - \Omega_i HDw_i\right|\right|^2 \right.$$
$$\left. + \frac{\nu}{2} \sum_{i=1}^{M} \left|\left|\exp(-\hat{z}_i) - w_i + v_i\right|\right|^2 \right\} \text{ s.t. } |\Omega_{i,k,k}| = 1 \tag{16}$$

Algorithm 1 RECONSTRUCTION

1: **for all** k in 1 to K_{max} **do**
2: THE TOMOGRAPHIC INVERSION STEP -

$$\hat{x} \leftarrow \underset{x\geq 0}{\operatorname{argmin}} \left\{ \frac{\mu}{2} \sum_{i=1}^{M} \left|\left|\hat{z}_i - u_i - A_i x\right|\right|^2 + R(x) \right\} \tag{13}$$

3: **for all** l in 1 to L_{max} **do**
4: ESTIMATING THE COMPLEX EXPONENTIAL -

$$\hat{z} \leftarrow \underset{z}{\operatorname{argmin}} \left\{ \frac{\mu}{2} \sum_{i=1}^{M} \left|\left|A_i\hat{x} - z_i + u_i\right|\right|^2 \right.$$
$$\left. + \frac{\nu}{2} \sum_{i=1}^{M} \left|\left|\exp(-z_i) - \hat{w}_i + v_i\right|\right|^2 \right\}. \tag{14}$$

5: PHASE RETRIEVAL STEP -

$$\hat{w} \leftarrow \underset{w}{\operatorname{argmin}} \left\{ \frac{1}{2\sigma^2} \sum_{i=1}^{M} \left|\left|y_i - \left|HDw_i\right|\right|\right|^2 \right.$$
$$\left. + \frac{\nu}{2} \sum_{i=1}^{M} \left|\left|\exp(-\hat{z}_i) - w_i + v_i\right|\right|^2 \right\}. \tag{15}$$

6: $v_i \leftarrow v_i + (\exp(-\hat{z}_i) - \hat{w}_i)$
7: **end for**
8: $u_i \leftarrow u_i + (A_i\hat{x} - \hat{z}_i)$
9: **end for**

To solve (16), we will alternately minimize over w and Ω till convergence is achieved. Since (16) is quadratic in w, the minimization over w is solved using the steepest-descent algorithm [17]. The minimization over Ω_i is separable in each of its diagonal elements and reduces to the problem of computing projections onto a circle with unit radius.

5. SIMULATION RESULTS

In this section, we compare CRITIR with the conventional approach to reconstruction in the limit of the near-field approximation. Under the near-field assumption, if the width of the smallest feature that is resolved is a, then the Fresnel number defined as, $N_F = a^2/(\lambda R)$, is assumed to be much larger than unity. If this assumption does not hold, it means that even if the detector is capable of resolving a feature with width a, it cannot be resolved by an algorithm that makes the near-field approximation. One such widely used method in the near-field is the Paganin's phase retrieval method that assumes that the object is composed of a single homogeneous material embedded in a material with negligible attenuation. Here, the phase is retrieved from the measured image at each view of the object using Paganin's phase retrieval [4] and the object is reconstructed by filter back-projection [18] of the retrieved phase images.

We generated a phantom ground-truth of size $N_u \times N_v \times N_w = 128 \times 512 \times 512$ with a voxel width of 0.175μm. The phantom consists of three latex spheres [4] with aver-

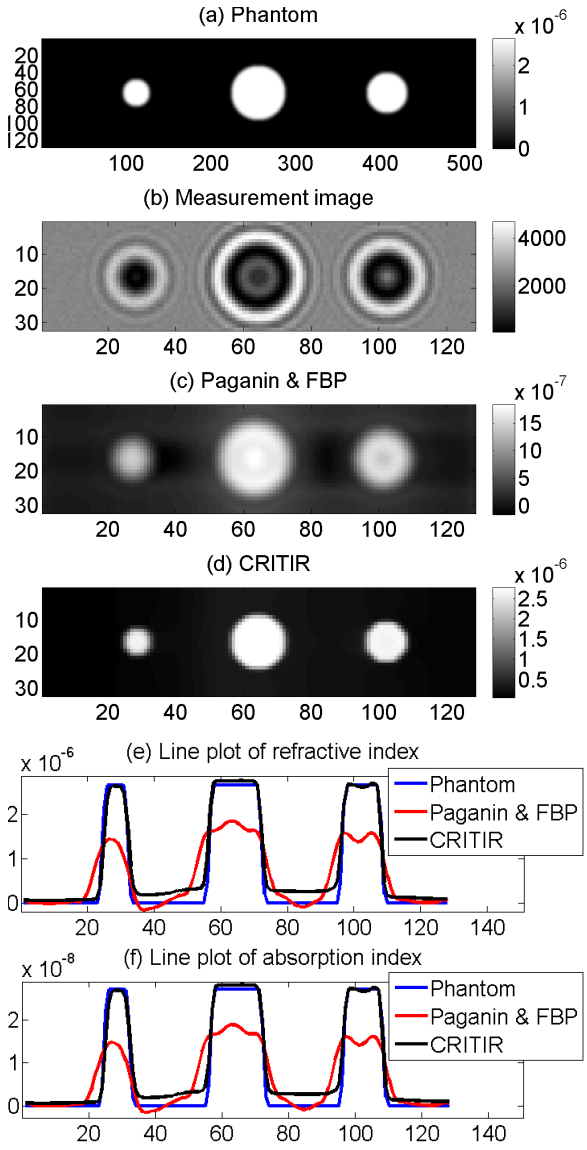

Fig. 1. (a) is the phantom ground-truth. (b) is the measured image at the detector. (c) is the FBP reconstruction of Paganin's phase retrieved images. (d) is the reconstruction using CRITIR. (e) and (f) are line plots of the refractive index decrement and absorption index respectively through the center of all three spheres. (a-d) correspond to the same 2D slice along the $u-$axis (vertical axis) and $v-$axis (horizontal axis). CRITIR accurately reconstructs the object while Paganin with FBP results in blurry edges and artifacts.

age values of $\beta = 2.7218 \times 10^{-08}$ for the absorption and $\delta = 2.6639 \times 10^{-06}$ for the refractive index decrement embedded in a material with negligible absorption and refraction. A slice of the phantom along the $u - v$ axes is shown in Fig. 1 (a). The measurement data is generated for a detector of size $N_u \times N_v = 32 \times 128$ by simulating the physics of X-ray propagation at an energy of 3keV, object to detector distance of $R = 400$mm, and $\gamma = 0.5898\mu\text{m}^{-1}$ in (4). The

Table 1. Root mean square error comparison

Description	Refractive index decrement, δ	Absorption index, β
Paganin & FBP	1.7850×10^{-7}	1.8100×10^{-9}
CRITIR	1.1705×10^{-7}	1.1938×10^{-9}

noise variance is equal to the simulated measurement value, where we assume an average photon count of 2500 for unattenuated projections. This leads to an average SNR of 35dB. A measured image along the $u - v$ axes is shown in Fig. 1 (b).

The absorption and refractive index decrement values of the object are reconstructed from measurements at 128 view angles. The reconstructions have a size of $N_u \times N_v \times N_w = 32 \times 128 \times 128$ and a voxel width of 0.7μm. In Fig. 1 (c-e), we compare the reconstructions of the refractive index decrement using CRITIR with the traditional approach of Paganin's phase retrieval followed by FBP reconstruction. A $u - v$ slice of the reconstruction using Paganin phase retrieval and FBP is shown in Fig. 1 (c). For CRITIR, we used the reconstruction obtained using Paganin and FBP as an initial estimate to avoid converging to a local minima due to the non-convex nature of (11). We set $\alpha = 98$ and $\sigma_-/\sigma_+ = 0.1$ in the prior model shown in (9). The regularization parameter σ_+ is adjusted to get the best subjective trade off between edge resolution and noise reduction. A $u - v$ slice of the reconstruction using CRITIR is shown in Fig. 1 (d). Fig. 1 (e, f) show a line plot of the refractive index decrement and absorption index through the center of the three spheres. For comparison purposes, the phantom line plot in Fig. 1 (e, f) is downsampled to the reconstruction resolution. We can see that the reconstruction of edges is much sharper and more accurate with CRITIR when compared to that with Paganin and FBP. CRITIR also dramatically improves the overall reconstruction quality by increasing resolution and reducing artifacts. The root mean square error between the reconstructions and the phantom for different algorithms is shown in table (1).

6. CONCLUSIONS

We presented a new algorithm called CRITIR that reconstructs the complex refractive index using a physics based model for X-ray propagation and a sparsity enforcing prior model for the object. Unlike traditional methods, CRITIR does not make simplifying approximations beyond the assumption of Fresnel diffraction. We generated simulated data beyond the near-field region and showed that CRITIR accurately reconstructs the object while the conventional approach results in excessive blurring of edges and reconstruction artifacts. CRITIR will enable a new generation of experiments that was not possible until now due to various limitations imposed by the conventional reconstruction methods.

7. REFERENCES

[1] A. Burvall, U. Lundström, Per A. C. Takman, D. H. Larsson, and H. M. Hertz, "Phase retrieval in X-ray phase-contrast imaging suitable for tomography," *Opt. Express*, vol. 19, no. 11, pp. 10359–10376, May 2011.

[2] A. V. Bronnikov, "Reconstruction formulas in phase-contrast tomography," *Optics Communications*, vol. 171, no. 46, pp. 239 – 244, 1999.

[3] T. E. Gureyev, T. J. Davis, A. Pogany, S. C. Mayo, and S. W. Wilkins, "Optical phase retrieval by use of first Born and Rytov-type approximations," *Appl. Opt.*, vol. 43, no. 12, pp. 2418–2430, Apr 2004.

[4] D. Paganin, S. C. Mayo, T. E. Gureyev, P. R. Miller, and S. W. Wilkins, "Simultaneous phase and amplitude extraction from a single defocused image of a homogeneous object," *Journal of Microscopy*, vol. 206, no. 1, pp. 33–40, 2002.

[5] X. Wu, H. Liu, and A. Yan, "X-ray phase-attenuation duality and phase retrieval," *Opt. Lett.*, vol. 30, no. 4, pp. 379–381, Feb 2005.

[6] M.A. Beltran, D.M. Paganin, K. Uesugi, and M.J. Kitchen, "2D and 3D X-ray phase retrieval of multi-material objects using a single defocus distance," *Opt. Express*, vol. 18, no. 7, pp. 6423–6436, Mar 2010.

[7] S. C. Mayo, P. R. Miller, S. W. Wilkins, T. J. Davis, D. Gao, T. E. Gureyev, D. Paganin, D. J. Parry, A. Pogany, and A. W. Stevenson, "Quantitative X-ray projection microscopy: phase-contrast and multi-spectral imaging," *Journal of Microscopy*, vol. 207, no. 2, pp. 79–96, 2002.

[8] S. Boyd, N. Parikh, E. Chu, B. Peleato, and J. Eckstein, "Distributed optimization and statistical learning via the alternating direction method of multipliers," *Foundations and Trends in Machine Learning*, vol. 3, no. 1, pp. 1–122, 2011.

[9] J. Baruchel, J.-Y. Buffière, E. Maire, P. Merle, and G. Peix, *X-Ray Tomography in Material Science*, Hermes Science Publications, 2000.

[10] K. A. Mohan, S.V. Venkatakrishnan, J.W. Gibbs, E.B. Gulsoy, X. Xiao, M. De Graef, P.W. Voorhees, and C.A. Bouman, "TIMBIR: A method for time-space reconstruction from interlaced views," *Computational Imaging, IEEE Transactions on*, vol. 1, no. 2, pp. 96–111, June 2015.

[11] N. L. Johnson, A. W. Kemp, and S. Kotz, *Univariate discrete distributions*, vol. 444, John Wiley & Sons, 2005.

[12] J.-B. Thibault, K. D. Sauer, C. A. Bouman, and J. Hsieh, "A three-dimensional statistical approach to improved image quality for multislice helical CT," *Medical Physics*, vol. 34, no. 11, pp. 4526–4544, 2007.

[13] K. A. Mohan, S.V. Venkatakrishnan, J.W. Gibbs, E.B. Gulsoy, X. Xiao, M. De Graef, P.W. Voorhees, and C.A. Bouman, "4D model-based iterative reconstruction from interlaced views," in *Acoustics, Speech and Signal Processing (ICASSP), 2015 IEEE International Conference on*, April 2015, pp. 783–787.

[14] K. A. Mohan, S.V. Venkatakrishnan, L.F. Drummy, J. Simmons, D.Y. Parkinson, and C.A. Bouman, "Model-based iterative reconstruction for synchrotron X-ray tomography," in *Acoustics, Speech and Signal Processing (ICASSP), 2014 IEEE International Conference on*, May 2014, pp. 6909–6913.

[15] J. W. Gibbs, K. A. Mohan, E. B. Gulsoy, A. J. Shahani, X. Xiao, C. A. Bouman, M. De Graef, and P. W. Voorhees, "The three-dimensional morphology of growing dendrites," *Nature Scientific Reports*, vol. 5, no. 11824, Jul 2015.

[16] J. C. Lagarias, J. A. Reeds, M. H. Wright, and P. E. Wright, "Convergence properties of the Nelder-Mead simplex method in low dimensions," *SIAM Journal on Optimization*, vol. 9, no. 1, pp. 112–147, 1998.

[17] E. Chong and S. H. Zak, *An introduction to optimization*, vol. 76, John Wiley & Sons, 2013.

[18] A. C. Kak and M. Slaney, *Principles of Computerized Tomographic Imaging*, Society for Industrial and Applied Mathematics, Philadephia, PA, 2001.